DNS CODE VALIDATION FOR COMPRESSIBLE SHEAR FLOWS USING LST

Jônatas Ferreira Lacerda, jonatasflacerda@hotmail.com
Leandro Franco de Souza, lefraso@icmc.usp.br
Josuel Kruppa Rogenski, josuelkr@gmail.com
Institute of Mathematical and Computer Sciences, University of São Paulo. São Carlos-SP, Brazil.

Márcio Teixeira de Mendonça, marciomtm@iae.cta.br
Instituto de Aeronáutica e Espaço, Divisão de Propulsão, São José dos Campos, SP, Brazil

Abstract.
In order to simulate compressible shear flow stability and aeroacoustic problems, a numerical code must be able to capture how a baseflow behaves when submitted to known small disturbances. If the disturbances are amplified the flow is unstable. The Linear Stability Theory (LST) provides a framework to obtain information about the growth rate in relation to the excitation frequency for a given base flow. The correspondent eigenfunction when used for disturbance introduction on direct numerical simulations (DNS) should capture the same growth rate. In the present work, DNS simulations of a two-dimensional compressible mixing layer and a two-dimensional compressible plane jet are performed. Disturbances are introduced at the domain inflow and the spatial growth rate obtained with a DNS code are compared with growth rates obtained from a LST analysis for each baseflow in order to verify and validate the DNS code. The good comparisons between the DNS simulations and LST results indicate that the code is able to simulate compressible flow problems and it is possible to use it to perform direct numerical simulation of instability and aeroacoustics problems.

Keywords: *compressible flow, direct numerical simulations, linear stability theory, code validation*

1. INTRODUCTION

There is an increasing concern about health problems related to noise in many engineering areas. Some noise sources are due to turbulence in a flow field and aeroacoustics is the area responsible for the investigation of noise generation and propagation by flow (aerodynamic noise). The problem of flow generated noise have some specific characteristics [9]: multiple frequencies, multiple scales and propagation to long distances with very low dissipation. To deal with these characteristics a numerical simulation must [9]: have a transient numerical scheme, have very low numerical dissipation and dispersion to preserve the propagation of acoustic waves and have non-reflecting boundary conditions when the physical domain is truncated to form the computational domain.

Along the years many studies has been conducted in the area of Computational Aeroacoustics (CAA). Two main approaches can be identified: The first one rely on acoustic analogies ([6], [7], [2],[3]) where noise sources are obtained from CFD results and its propagation are calculated solving an inhomogeneous wave equation for pressure subjected to these sources. The second approach uses a high fidelity simulation capable of computing directly the acoustic waves together with the fluid flow, which is called direct numerical simulation (DNS) of aeroacoustics.

In order to be able to perform DNS of aeroacoustic problems in the future, a numerical code was developed within our research group. It uses parallel processing with domain decomposition to perform the calculations in a feasible time. High order temporal and spatial discretization schemes were adopted to minimize the dispersion and dissipation phenomena on the simulation of the flow field and of the acoustics waves. A series of strategies such as filtering and mesh stretching as well as characteristic boundary conditions were implemented in order to obtain a proper solution of the aeroacoustics problem.

However, before using this code for aeroacoustic predictions, it is necessary to verify and validate it and see if the code is able to capture the flow behaviour when submitted to known small disturbances. The Linear Stability Theory (LST) provides a framework to obtain information about the amplification rate in relation to the excitation frequency and the corresponding eigenfunctions. The results from LST can be used for comparisons with DNS simulations.

In the present work results are presented for DNS simulations of a two-dimensional compressible mixing layer and two-dimensional compressible plane jet. Disturbances were introduced at the domain inflow and the code verification was done by comparing the spatial amplification rate obtained by the DNS code with amplification rates obtained from a LST analysis of each base flow. The good comparison obtained indicated that the code can simulate compressible flow problems and it is possible to use it to perform direct numerical simulation of aeroacoustics problems.

2. FORMULATION AND NUMERICAL SCHEME

The code was developed to solve the two-dimensional unsteady compressible Navier-Stokes equations together with the continuity and energy equations in the dimensionless form ([5]). A perfect gas relation for pressure is assumed to close the problem. In the conservative form, the unknowns are given by the density ρ, momentum densities ρu, ρv and total energy E.

Time integration is performed using a 4th-order 4-steps Runge-Kutta scheme. The spatial discretization in the streamwise x and normal y directions is done by a 6th-order compact finite difference method and the generated tridiagonal equation systems are solved using the Thomas algorithm (TDMA).

An non-uniform x, y grid is used, as shown in Fig. 3. An interest region with uniform grid is delimited. Then, a grid stretching of approximately 1% is applied in both directions that, together with spatial low-pass filtering, creates a damping zone. Disturbances become increasingly badly resolved and dissipated as they propagate through the damping zone before they reach the outflow boundaries.

The code was parallelized through domain decomposition in both directions using shared-memory parallelization and MPI libraries are used for inter nodal communications. A grid transformation in the (x, y) plane is used to map the physical grid in a equidistant (ξ, η) computational grid, and metrics are necessary for the derivative calculations. The first derivatives are given by:

$$\frac{\partial}{\partial x} = \frac{1}{\left(\frac{\partial x}{\partial \xi}\right)}\frac{\partial}{\partial \xi}, \tag{1}$$

$$\frac{\partial}{\partial y} = \frac{1}{\left(\frac{\partial y}{\partial \eta}\right)}\frac{\partial}{\partial \eta}. \tag{2}$$

Second derivatives are:

$$\frac{\partial^2}{\partial x^2} = \frac{1}{\left(\frac{\partial x}{\partial \xi}\right)^2}\frac{\partial^2}{\partial \xi^2} - \frac{\frac{\partial^2 x}{\partial \xi^2}}{\left(\frac{\partial x}{\partial \xi}\right)^3}\frac{\partial}{\partial \xi} = \frac{\partial^2}{\partial \xi^2}\left(\frac{\partial \xi}{\partial x}\right)^2 - \frac{\partial}{\partial \xi}\frac{\partial^2 \xi}{\partial x^2}, \tag{3}$$

$$\frac{\partial^2}{\partial y^2} = \frac{1}{\left(\frac{\partial y}{\partial \eta}\right)^2}\frac{\partial^2}{\partial \eta^2} - \frac{\frac{\partial^2 y}{\partial \eta^2}}{\left(\frac{\partial y}{\partial \eta}\right)^3}\frac{\partial}{\partial \eta} = \frac{\partial^2}{\partial \eta^2}\left(\frac{\partial \eta}{\partial y}\right)^2 - \frac{\partial}{\partial \eta}\frac{\partial^2 \eta}{\partial y^2}, \tag{4}$$

where the metrics are given by:

$$\frac{\partial^2 \xi}{\partial x^2} = -\frac{\partial^2 x}{\partial \xi^2}\left(\frac{\partial \xi}{\partial x}\right)^3, \tag{5}$$

$$\frac{\partial^2 \eta}{\partial y^2} = -\frac{\partial^2 y}{\partial \eta^2}\left(\frac{\partial \eta}{\partial y}\right)^3. \tag{6}$$

Special boundary conditions are used to avoid disturbance reflection from boundaries. For the inflow, characteristics are used and for the free stream and outflow boundaries null derivative of the properties are used. Together with grid stretching and low-pass filtering, they dissipate the disturbances before they reach the boundaries.

Inviscid linear stability theory analysis was used to obtain the frequency with maximum spatial growth rate and the correspondent eigenfunctions are introduced as disturbances at the simulation inflow boundary.

3. RESULTS

3.1 Compressible two-dimensional mixing layer

A compressible mixing layer consists of two streams with different velocities flowing parallel to one another such that the resulting velocity profile assumes an “S” shape. Due to the inflectional point on the velocity profile, the flow is unstable and transition to turbulence due to the generation and growth of vortical structures. For the present verification, the flow configuration has been closely matched to the case investigated by [1].

The Mach numbers of the upper and the lower streams are $Ma_1 = 0.50$ and $Ma_2 = 0.25$, respectively. The Reynolds number is 500 and is based on the vorticity thickness at the inflow. The inflow velocity, density and temperature profiles are showed in Fig. 1 and are obtained by solving the steady compressible two-dimensional boundary-layer equations.

The eigenfunctions used to introduce the disturbances at the DNS inflow boundary were obtained from a spatial viscous linear stability analysis, where the fundamental frequency is $\omega_{=}0.62930$. The corresponding eigenfunction amplitude and

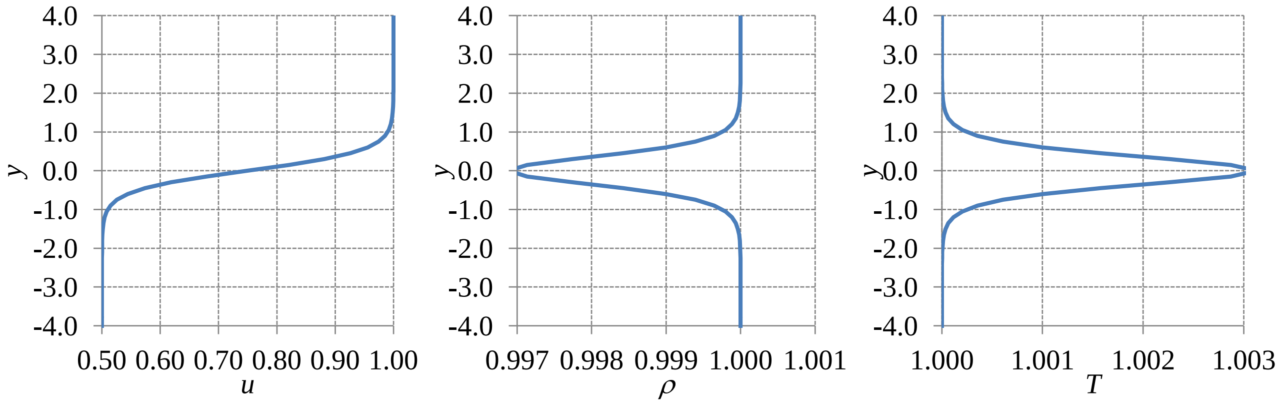

Figure 1. Inflow profile for velocity u, density and temperature for the 2D mixing layer.

phase are shown in Fig. 2. This and three subharmonics were used to disturb the flow. The maximum amplitude of the fundamental frequency is 0.002 while for the other subharmonics the maximum amplitude is 0.001, all normalized by the correspondent maximum u velocity amplitude. Furthermore, a phase shift of $\Delta\theta = -0.028$ was introduced for the first subharmonic, $\Delta\theta = 0.141$ for the second and $\Delta\theta = 0.391$ for the third.

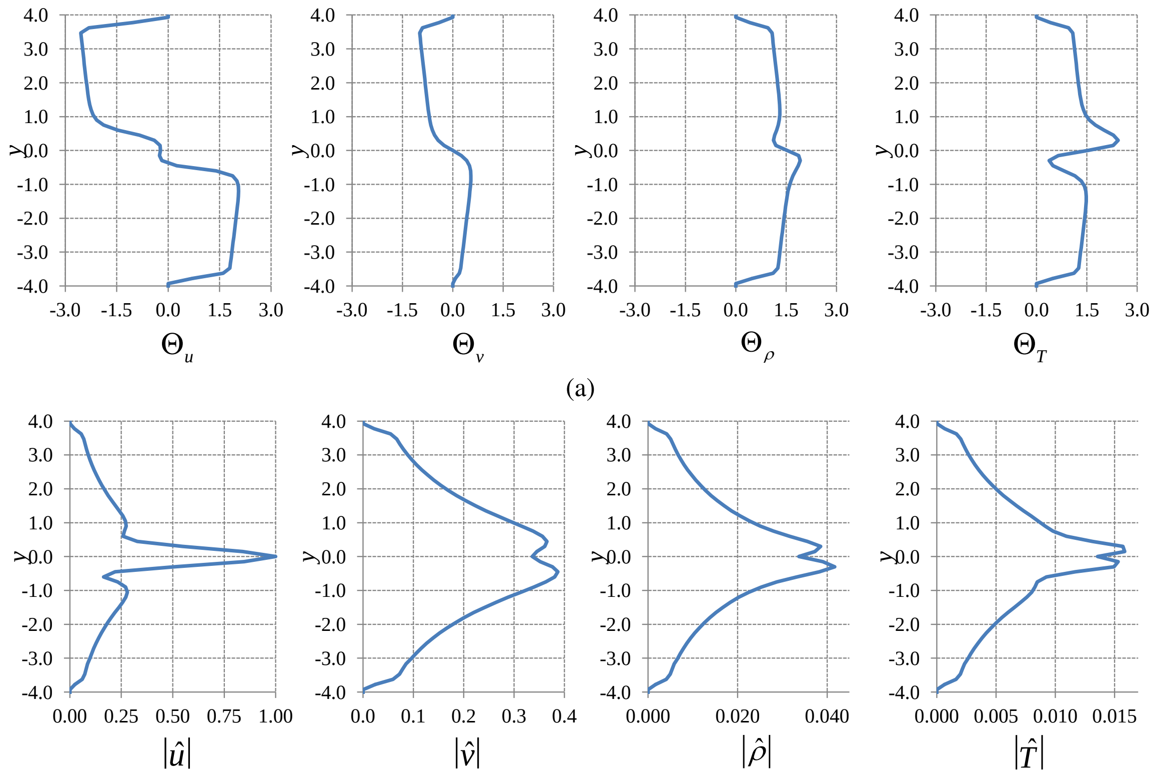

Figure 2. (a) amplitude and (b) phase distribution for the 2D mixing layer.

A representation of the computational mesh, showing the domain regions and boundary conditions, is presented in Fig. 3. A computational mesh with 2500 x 850 points in the x and y directions was used. In the longitudinal direction the mesh has constant increment $\Delta x = 0.157$ up to $x = 300$, forming the region of interest and downstream the mesh is stretched with a rate of approximately 1.0%, forming a damping zone. In the normal direction the mesh is stretched from the center to the boundaries, with the lowest increment of $\Delta y = 0.15$ and the highest increment of $\Delta y = 1.06$.

As inflow boundary conditions, the u velocity, temperature and density profiles presented in Fig. 1 were used. The disturbances were introduced at each step of the Runge-Kutta. Furthermore, characteristic boundary conditions are used at the inflow to avoid reflections of outgoing waves back to the computational domain. To minimize reflections caused by oblique acoustic waves, a damping zone is applied at the upper and lower boundary, forcing the flow variables to a steady state solution. To avoid large structures flowing through the outflow boundary, a combination of grid stretching

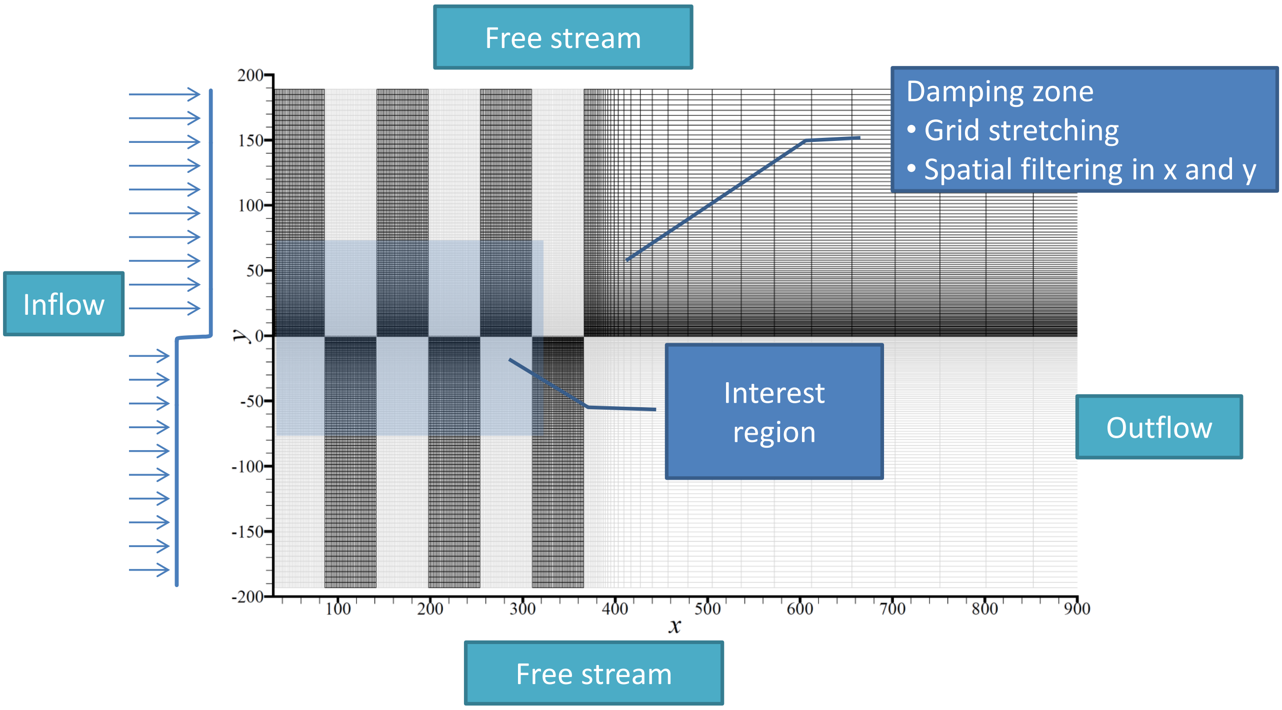

Figure 3. Computational domain detaching the interest region, the damping zone and the boundaries for 2D mixing layer.

and spatial low-pass filtering are applied in the damping zone. Thus, disturbances become increasingly badly resolved as they propagate through this region and by applying a spatial filter, the perturbations are substantially dissipated before they reach the outflow boundary.

The chosen time-step was $\Delta t = \frac{2\pi}{\omega \cdot n_{\text{steps}}}$, where n_{steps} is the number of points per wavelength of the fundamental frequency. In this case, $n_{\text{steps}} = 752$, corresponding to a time-step $\Delta t = 0.0133$. Seventy six periods of the fundamental frequency were simulated and the last eight were chosen for post-processing analysis.

The observation of the maximum amplitude of the normal velocity v along the $y-$direction for each x position can show how the disturbances are growing in the domain, as shown in Fig. 4. In the initial part of the domain the amplitudes grow exponentially until non-linear effects are observed, causing a saturation of the maximum amplitude of v.

The spatial growth rate α_i, calculated by Eq. 7, can be compared with results from linear stability theory, as shown in Fig. 5. Table 1 presents the difference between DNS and LST results, where there is an initial portion of the domain with an elevated error due the receptivity of the flow to the disturbances near the inflow. Further downstream (after $x \approx 45$) the differences decrease and the maximum difference was 4% for mode (1,0), 9% for mode (1/2,0) and 15% for mode (1/4,0). Although α_i is a very sensitive value, mainly for the subharmonics, the mean values of the DNS corresponded well to those predicted by linear stability theory. Thus, the good agreement between simulation and theory serves as a verification of the implemented DNS computational code for small disturbances.

$$\alpha_i = -\frac{\partial}{\partial x}\left[\ln\left(|v|_{\max}\right)\right]. \tag{7}$$

Besides the spatial amplification rate comparison, the transversal vorticity Ω_z at the end of the simulation were compared with the results presented by [1] as shown in Fig. 6. It is possible to see the formation of the first Kelvin-Helmholtz vortices which pair downstream forming new structures. A good match with [1] was obtained.

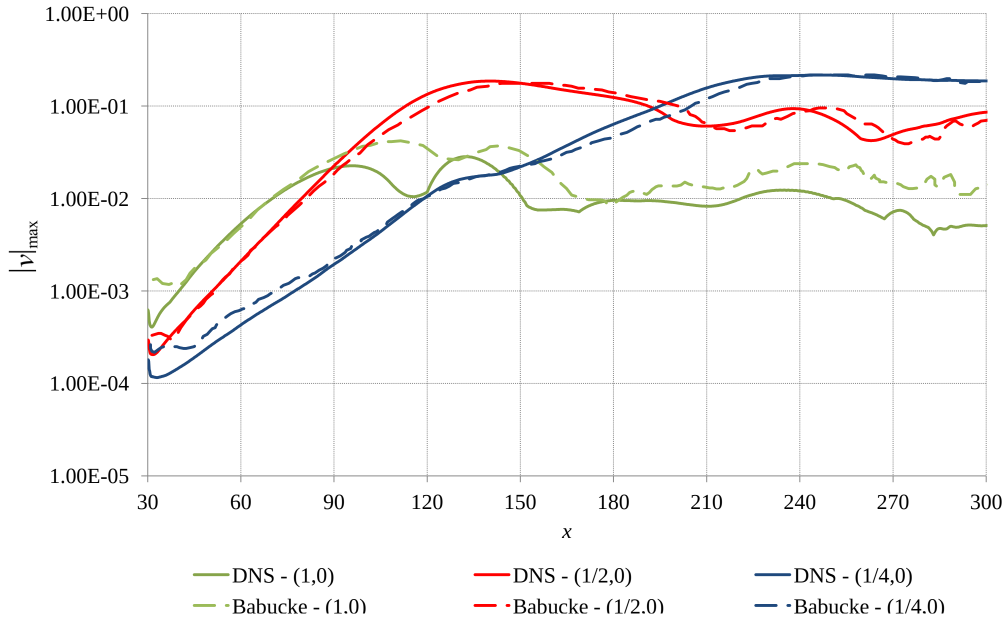

Figure 4. Maximum amplitude of the normal velocity v along the $y-$direction for each x position comparison with results from [1].

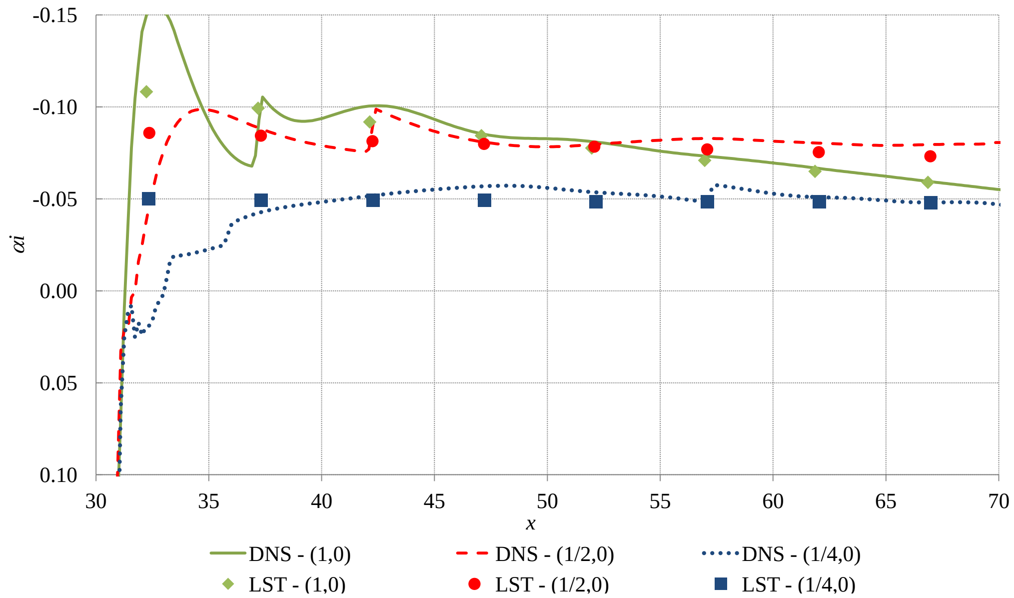

Figure 5. Spatial amplification rate comparison between LST and DNS for the 2D mixing layer.

Table 1. Spatial amplification rate comparison between LST and DNS for the 2D mixing layer.

	(1,0)			**(1/2,0)**			**(1/4,0)**		
x	**LST**	**DNS**	**%**	**LST**	**DNS**	**%**	**LST**	**DNS**	**%**
32	-0.108	-0.155	43%	-0.086	-0.046	-46%	-0.05	0.0189	-138%
37	-0.099	-0.093	-6%	-0.084	-0.088	5%	-0.049	-0.042	-14%
42	-0.092	-0.101	10%	-0.081	-0.089	9%	-0.049	-0.052	5%
47	-0.084	-0.085	1%	-0.08	-0.081	1%	-0.049	-0.057	15%
52	-0.078	-0.081	4%	-0.078	-0.08	2%	-0.049	-0.054	10%
57	-0.071	-0.073	3%	-0.077	-0.083	8%	-0.049	-0.048	0%
62	-0.065	-0.067	2%	-0.075	-0.08	7%	-0.049	-0.051	5%
67	-0.059	-0.059	1%	-0.073	-0.079	9%	-0.048	-0.048	1%

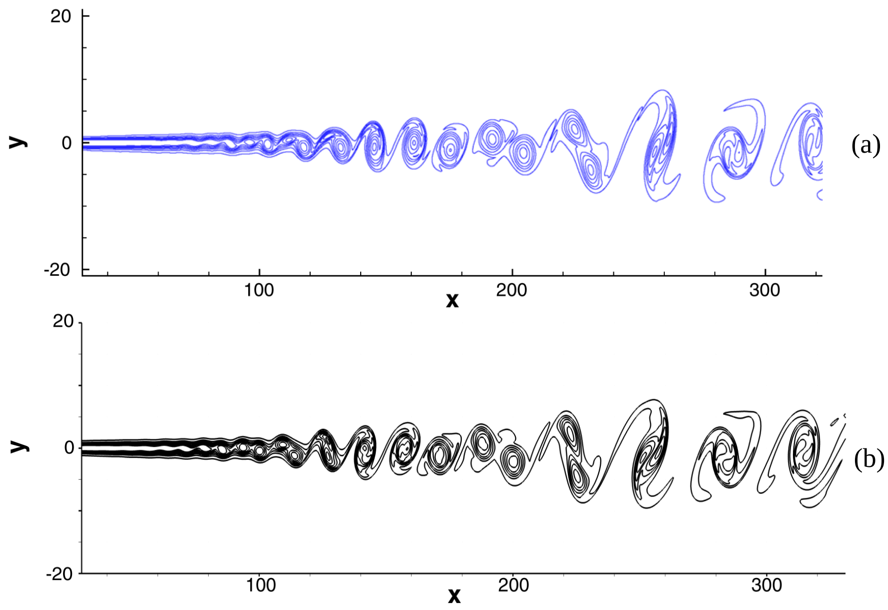

Figure 6. Transversal vorticity at final time-step. Contour levels from -0.26 up to 0.02 with an increment of 0.04. (a) results from [1] and (b) DNS code.

3.2 Compressible two-dimensional plane jet

Plane jets are a typical shear flow present in several applications such as in combustion and propulsion. The interest in aerodynamic noise generated by jets is growing fast in the aeronautical industry. In this flow, a central core with high velocity mixes with a parallel stream with lower velocity. In the interface between both flow streams there is high gradients of the flow properties, making the flow unstable to disturbances. In the present investigation a two-dimensional plane jet was studied. The inflow velocity profile is given by:

$$u\left(y\right)=\frac{\mathrm{Ma}_j-\mathrm{Ma}_\infty}{\mathrm{Ma}_j+\mathrm{Ma}_\infty}\tanh\left[2\left(y+\theta\right)\right]+1, \tag{8}$$

where $\theta=1.98$ and the velocity profile is symmetric with respect to $y=0$ as shown in Fig. 7. The ratio between the jet and the far field co-flow was kept equal to $U_j/U_\infty=1.67$ for all cases. The jet is perfectly expanded and isothermal such that the temperature, density and pressure profiles are kept constant. The Prandtl number is $\mathrm{Pr}=0.71$. Since the linear stability analysis is inviscid, the DNS simulations are done with a high Reynolds number ($\mathrm{Re}=10000$) such that the inertia effects are much higher than the viscous effects.

A computational Cartesian grid with 1400 x 800 nodes in x and y directions was used in all simulations. In the longitudinal direction the grid is uniform with $\Delta x=0.25$ up to $x\approx 250$ and than stretched at a 1.0% rate. In the normal direction, there is also a uniform grid with $\Delta y=0.106$ up to $y\approx\pm 5.20$ and then stretched at a 1.0% rate. The uniform spacing zone corresponds to the interest zone, while the stretched grid region corresponds to the damping zone. Domain decomposition was adopted to parallel the computation.

For boundary conditions, at inflow the u velocity component is given by Eq. 8. As in the two-dimensional mixing layer case, the disturbances were introduced at each step of the Runge-Kutta scheme and the necessary numerical cares adopted to avoid numerical contamination of the solution was also used.

The chosen time step was $\Delta t=\frac{2\pi}{\omega\cdot n_{\mathrm{steps}}}$, where n_{steps} is the number of points per wavelength of the fundamental frequency. The number of time steps used by fundamental frequency was $n_{\mathrm{steps}}=752$. In each case 76 periods were simulated for the fundamental frequency, where the last 8 were chosen to post-processing analysis.

Compressible jet stability results are know to have two possible modes, a varicose mode and a sinuous mode. An inviscid LST analysis was performed considering only the varicose mode. A classic normal modes analysis using the Gropengiesser [4] formulation was performed, where a new variable ξ is defined combining both p and v disturbance eigenfunctions as

$$\xi=\frac{i\alpha p}{\gamma Ma^2 v} \tag{9}$$

$$g=\frac{\alpha^2+\beta^2}{\rho\alpha^2}-Ma^2\frac{(\alpha U-\omega)^2}{\alpha^2}, \tag{10}$$

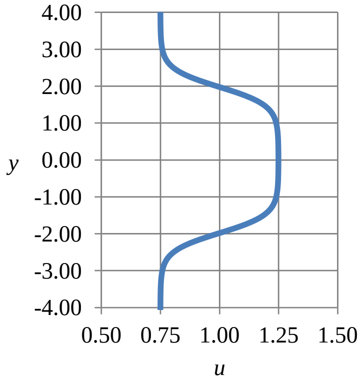

Figure 7. u-velocity profile for the 2D plane jet.

resulting in the following form of the Rayleigh stability equation ([8]).

$$\xi' = \rho\alpha(\alpha U - \omega) - \frac{\alpha\xi}{\alpha U - \omega}(g\xi - U'). \tag{11}$$

Where α and ω are the streamwise wave number and frequency.

The simulated cases and their correspondent maximum spatial amplification rate and frequency are presented in Tab. 2. The corresponding jet, free-stream and convective Mach numbers $(\mathrm{Ma}_j, \mathrm{Ma}_\infty,$ and $\mathrm{Ma}_c)$ are shown on the table.

$$\mathrm{Ma}_c = \frac{\mathrm{Ma}_j - \mathrm{Ma}_\infty}{2}. \tag{12}$$

Table 2. Mach numbers and maximum spatial amplification rates.

Case	Ma_j	Ma_∞	Ma_c	ω_r	α_r	α_i
1	0.25	0.15	0.05	0.9036	0.8980	0.0933
2	1.05	0.63	0.21	0.8927	0.8875	0.0855
3	1.50	0.90	0.30	0.8740	0.8690	0.0773
4	2.00	1.20	0.40	0.8350	0.8301	0.0654
5	2.50	1.50	0.50	0.7636	0.7586	0.0507
6	3.00	1.80	0.60	0.6370	0.6311	0.0335

The variation of the spatial amplification rate with Ma_j is shown in Fig. 8. It is possible to observe that increasing the Mach number there is a decrease in the maximum value of the amplification rate, and the flow becomes more stable.

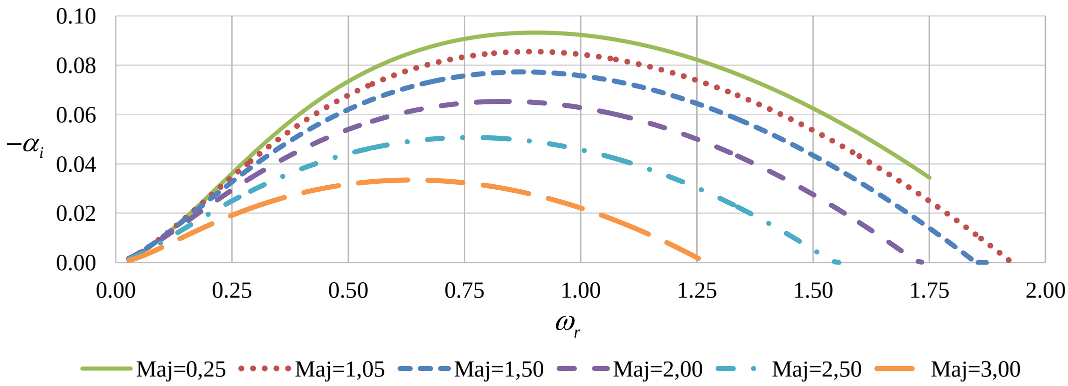

Figure 8. Spatial amplification rates for the 2D plane jet.

The decrease of the amplification rate and consequent mixing of the flow is a known effect. This effect is of great importance in combustion flows and can also help on noise control.

The maximum amplitude of the normal velocity v along the $y-$direction as a function of the streamwise x position ($|v|_{\max}$) are presented in Fig. 12. It is possible to identify an initial receptivity region of the disturbances near the inflow. Downstream occurs an exponential increase in the amplitude corresponding to linear growth effects up to a maximum level were non-linear effects become significant. As the flow becomes more stable with increasing Mach number, the x position where ($|v|_{\max}$) reaches a maximum is delayed to a position further downstream with the increase of the Mach number. A comparison with spatial amplification rates obtained by the LST analysis is also presented in Figs. 12. Except for the receptivity region close to the inflow, there is a good comparison between LST and DNS results. Again, it was possible to say that the good agreement between simulation and theory serves as a verification of the implemented DNS computational code for small disturbances.

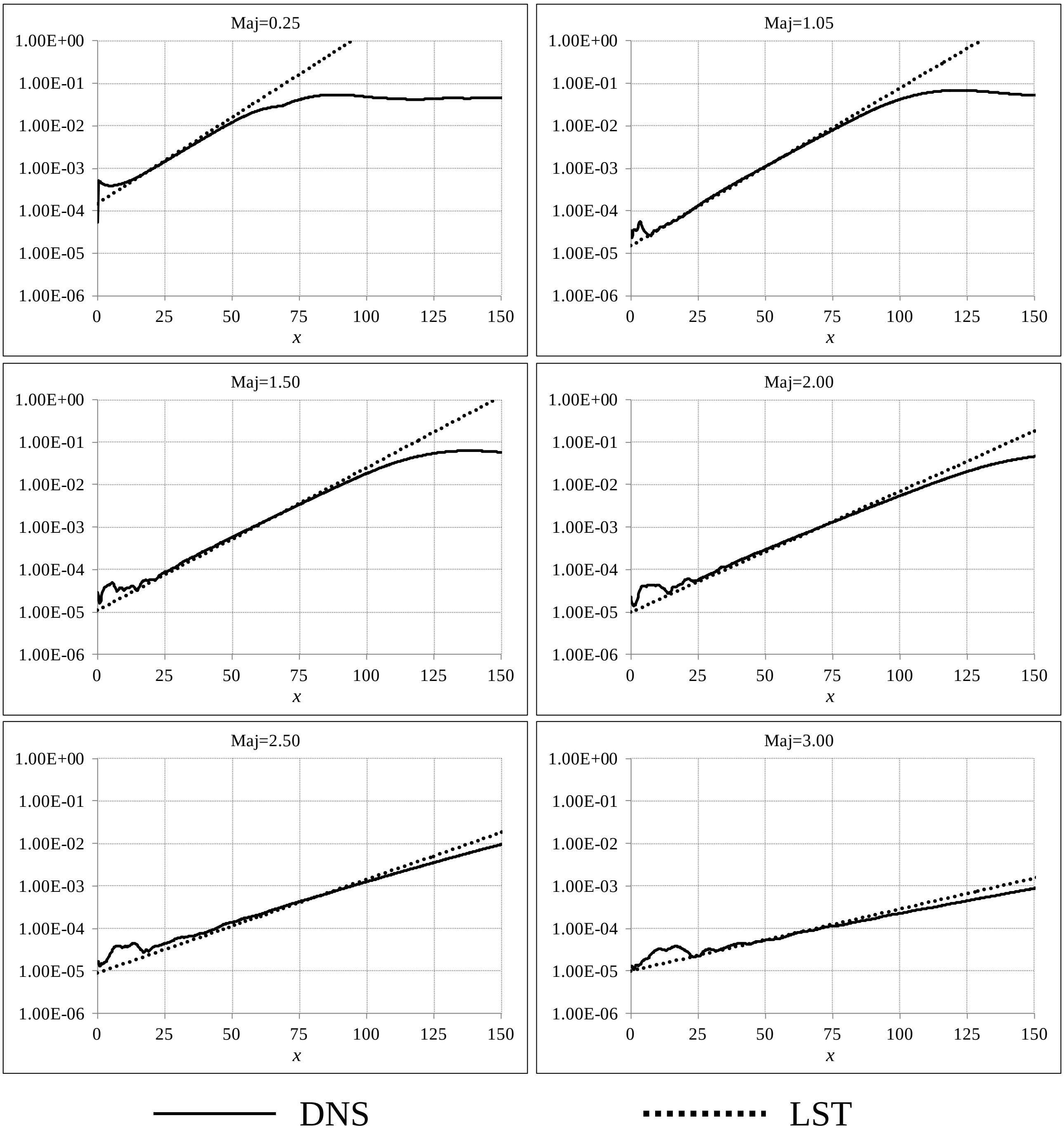

Figure 9. Maximum amplitude of the normal velocity v along the $y-$direction for each x position (DNS result) and comparison with LST spatial amplification rate.

4. SUMMARY

Two compressible shear flows has been simulated using a two-dimensional DNS code, a two-dimensional compressible mixing-layer and a two-dimensional compressible plane jet. The results have been compared with linear stability theory and very good agreement have been found, showing that the DNS code can simulate wave propagation phenomena with the necessary accuracy regarding dispersion and dissipation effects.

5. ACKNOWLEDGEMENTS

For their support, Tecumseh do Brasil Ltda. and National Council for Scientific and Technological Development (CNPq).

6. REFERENCES

Babucke, A. and Kloker M. and Rist U., 2008, "DNS of a Plane Mixing Layer for the Investigation of Sound Generation Mechanisms", Computers and Fluids, Vol.37, n.4, pp. 360-368.

Curle, N., 1955, "The Influence of Solid Boundaries upon Aerodynamic Sound", Proceedings of the Royal Society of London. Series A. Mathematical and Physical Sciences, Vol.231, n.1187, pp. 505-514.

Ffowcs-Williams, J.E. and Hawkings, D.L., 1969, "Sound Generation by Turbulence and Surfaces in Arbitrary Motion", Philosophical Transactions of the Royal Society of London. Series A. Mathematical and Physical Sciences, Vol.264, n.1151, pp. 321-342.

Gropengiesser, H., 1970, "Study on the stability of boundary layers in compressible fluids", Tech. Rep. NASA TT F-12, National Aeronautics and Space Administration–NASA.

Lacerda, J.F., 2016 "Aeroacústica Computacional através de Simulação Numérica Direta de Escoamentos Livres Cisalhantes Compressíveis", PhD Thesis, ICMC - USP, São Carlos-SP, Brazil

Lighthill, M.J., 1952, "On Sound Generated Aerodynamically. I. General Theory", Proceedings of the Royal Society of London. Series A. Mathematical and Physical Sciences, Vol.211, n.1107, pp. 564-587.

Lighthill, M.J., 1954, "On Sound Generated Aerodynamically. II. Turbulence as a Source of Sound", Proceedings of the Royal Society of London. Series A. Mathematical and Physical Sciences, Vol.222, n.1148, pp. 1-32.

Salemi, L. C., and Mendonca, M. T., 2008, "Spatial and Temporal Linear Stability Analysis of Binary Compressible Shear Layer", AIAA *38th Fluid Dynamics Conference*, AIAA paper 2008-3841, Seattle, USA.

Tam, C.K.W., 2004, "Computational Aeroacoustics: An Overview of Computational Challenges and Applications", Int. Journal of Computational Fluid Dynamics, Vol.18, n.6, pp.547-567.